Geophysical Prospecting, 2001, **49**, 165–178

Implementing the fast marching eikonal solver: spherical versus Cartesian coordinates

Tariq Alkhalifah* and Sergey Fomel†

Institute for Astronomy and Geophysical Research, King AbdulAziz City of Science and Technology (KACST), PO Box 6086, Riyadh 11442, Saudi Arabia

Received October 1999, revision accepted August 2000

ABSTRACT

Spherical coordinates are a natural orthogonal system for describing wavefronts emanating from a point source. A regular grid distribution in the Cartesian-coordinate system tends to undersample the wavefront description near the source (at the highest wavefront curvature) and oversample it away from the source. Spherical coordinates, in general, provide a more balanced grid distribution for characterizing point-source wavefronts. Our numerical implementation confirms that the recently introduced fast marching algorithm is both a highly efficient and an unconditionally stable eikonal solver. However, its first-order approximation of traveltime derivatives can induce relatively large traveltime errors for waves propagating in a diagonal direction with respect to the coordinate system. Examples, including the IFP Marmousi and the SEG/EAGE 3D salt-dome models, show that a spherical-coordinate implementation of the method results in far fewer errors in traveltime calculation than the conventional Cartesian-coordinate implementation, and with practically no loss in computational advantages.

INTRODUCTION

A recently introduced method for solving the eikonal equation, named the *fast marching* method (Sethian 1996; Sethian and Popovici 1999), has two very intriguing features: it is unconditionally stable and, at the same time, highly efficient. Essentially, the method is based on solving the eikonal equation on a Cartesian grid along the wavefront, starting with those points with minimum traveltime, an idea similar to the method of *expanding wavefronts* (Qin *et al.* 1992). Additionally, a minimum traveltime tree is constructed using fast algorithms (heap sorting) and this can be maintained at a computational cost proportional to $\log N$, where N is the number of gridpoints in the computational domain. As a result, the cost of the eikonal solver is approximately proportional to $N \log N$. The minimum-time requirement ensures the stability of the method, regardless of the complexity of the velocity model.

However, this new solver has a problem: it is based on a first-order approximation of the traveltime derivatives with respect to position. This low-order approximation can result in relatively large traveltime errors, particularly in two cases:

- when there is a large wavefront curvature, such as near the source;
- when the wavefront propagation is diagonal to the grid orientation.

Higher-order approximations of the traveltime derivatives could reduce these errors, but at an increased computational cost.

We investigate the possibility of reducing the computational errors by implementing the fast marching solver in spherical coordinates. The ability to handle turning waves is usually considered the main advantage of solving the eikonal equation in polar coordinates (Popovici 1991; van Trier and Symes 1991; Schneider 1993; Fowler 1994). Turning waves,

*E-mail: tkhalfah@kacst.edu.sa

†Now at: Stanford Exploration Project, Stanford University, 397 Panama Mall, Stanford, CA 94305, USA.E-mail: sergey@sep.stanford.edu

however, do not present a problem with this new scheme; the method can, by design, handle wavefronts at any angle, provided that they correspond to the first arrival. Nevertheless, the importance of the polar coordinates in the fast marching approach should not be underestimated. Compared with the Cartesian-coordinate implementation of the fast marching algorithm, in both simple and complex velocity models, we show that the polar-coordinate implementation can considerably improve the accuracy of the solution with practically no loss of computational efficiency.

FINITE-DIFFERENCE SOLUTION OF THE EIKONAL EQUATION

Using the high-frequency approximation, wavefronts in a 3D model can be described by the eikonal equation,

$$\left(\frac{\partial t}{\partial x}\right)^2+\left(\frac{\partial t}{\partial y}\right)^2+\left(\frac{\partial t}{\partial z}\right)^2=s^2(x,y,z), \tag{1}$$

where t is the traveltime, and s is the wave slowness in a 3D model. For arbitrary slowness models the eikonal equation can be solved numerically using finite-difference schemes, a method introduced by Vidale (1990).

Solving the eikonal equation numerically is probably the most efficient way of obtaining wavefront traveltimes in arbitrarily inhomogeneous media. One reason for the efficiency is that we can conveniently solve the eikonal equation over a regular grid, which eliminates the need for the interpolation commonly used with other methods, such as ray tracing.

A major drawback of using conventional methods to solve the eikonal equation numerically is that we evaluate only the fastest arrival solution, not necessarily the most energetic (Vidale 1990). This results in a less than acceptable traveltime computation for imaging in complex media (Geoltrain and Brac 1993). Another drawback of the eikonal solvers is that the conventional solvers are generally unstable in complex media (Popovici 1991). Stability usually requires the use of a finer, and hence more expensive, computational grid. In addition, conventional Cartesian-grid eikonal solvers cannot treat turning waves. The use of polar coordinates does not totally eliminate the turning wave problem, but it does allow for wavefronts to overturn at depth through a considerable angle, on the condition that they do not overturn on the radial axis.

The eikonal equation can also be described in spherical coordinates (r, θ and ϕ; see Fig. 1), as follows:

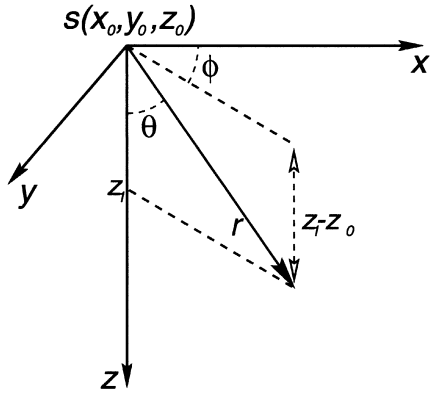

Figure 1 A spherical coordinate system given by r, θ and ϕ. The source $s(x_0, y_0, z_0)$ is at the origin of the spherical coordinates where $r = 0$. The parameter $r = \sqrt{(x-x_0)^2+(y-y_0)^2+(z-z_0)^2}$ is the distance from the source to the point of interest along the wavefront. The parameter ϕ is the angle between the x-axis and the projection of r on the $x-y$ plane. The parameter θ is the angle between the z-axis and r along a vertical plane.

$$\left(\frac{\partial t}{\partial r}\right)^2+\frac{1}{r^2}\left(\frac{\partial t}{\partial \theta}\right)^2+\frac{1}{r^2\sin^2\theta}\left(\frac{\partial t}{\partial \phi}\right)^2=s^2(r,\theta,\phi). \tag{2}$$

Note that $\sin\theta$ equals zero for vertical wave propagation, which poses a problem for this eikonal equation. However, the change of t with respect to ϕ is, in this case, meaningless. Therefore, a flag is necessary to remove the ϕ term when waves are propagating vertically or nearly vertically. A small constant parameter ($\approx\epsilon$) added to $\sin\theta$ in the denominator of the ϕ term will ensure numerical stability. Other stability solutions have been suggested by Schneider (1993) and Fowler (1994). In addition, the variation of the grid size in polar coordinates poses a problem for the stability of conventional solvers, especially when encountering small-scale inhomogeneities away from the source (Popovici 1991; Fowler 1994). These stability problems are eliminated by using the fast marching method, which is unconditionally stable. The spherical-coordinate system, as will be seen below, also helps to improve the accuracy of the fast marching method.

In 2D polar coordinates, we eliminate the ϕ terms so that the eikonal equation, described by r and θ, is given by

$$\left(\frac{\partial t}{\partial r}\right)^2+\frac{1}{r^2}\left(\frac{\partial t}{\partial \theta}\right)^2=s^2(r,\theta). \tag{3}$$

The only singularity in the polar-coordinate form occurs at $r = 0$ which is easily avoidable by placing the source at $r = 0$, and, therefore, setting the time t to zero at $r = 0$.

THE FAST MARCHING ALGORITHM

The fast marching method for numerically solving the eikonal equation has been described in detail by Sethian (1996) and a closely related method was used by Cao and Greenhalgh (1994). In this section, we give a summary of the approach, as well as indicating some of its advantages and drawbacks.

Starting from a point source (we can also start with a plane or any closed surface of sources), we calculate the traveltime at the surrounding gridpoints analytically. Obtaining initial analytical solutions is necessary in order to reduce some of the first-order numerical errors, discussed in detail below. The original point source is set; that is, its traveltime cannot be updated. The new traveltimes of the surrounding gridpoints are put into an array which constitutes the wavefront and are sorted from minimum to maximum traveltime values. The minimum traveltime, which is in the front of this array, is extracted first; its value is set (it cannot be updated in the future) and all neighbouring non-set gridpoints are updated using the following formula (Sethian 1996):

$$\begin{aligned}&\max(D_{ijk}^{-x}t,0)^2+\min(D_{ijk}^{+x}t,0)^2+\\&\max(D_{ijk}^{-y}t,0)^2+\min(D_{ijk}^{+y}t,0)^2+\\&\max(D_{ijk}^{-z}t,0)^2+\min(D_{ijk}^{+z}t,0)^2=s_{ijk}^2,\end{aligned}\tag{4}$$

where D_{ijk}^{-x} is the derivative of traveltime with respect to x at gridpoint (i, j, k) given by

$$D_{ijk}^{-x}t=\frac{t_{i,j,k}-t_{i-1,j,k}}{\Delta x}$$

and

$$D_{ijk}^{+x}t=\frac{t_{i+1,j,k}-t_{i,j,k}}{\Delta x}.$$

The abbreviations max and min in (4) correspond to the maximum and minimum, respectively, of the two variables separated by a comma within brackets. The same holds for D_{ijk}^{-y}, D_{ijk}^{+y}, and D_{ijk}^{-z}, D_{ijk}^{+z} for y and z, respectively. The traveltime t_{ijk} and the slowness s_{ijk} correspond to the gridpoint that is being updated. Solving for t_{ijk}, the time at a new gridpoint, requires solving a quadratic equation that has two solutions. We choose the solution that reduces to $t_{ijk}=t_{i-1,j,k}+\frac{\Delta x}{v}$, or $t_{ijk}=t_{i+1,j,k}+\frac{\Delta x}{v}$, when the wavefront travels horizontally, where v is the velocity at gridpoint (i, j, k). We repeat this for all other non-set points surrounding the initial extracted point. Each newly computed gridpoint is added to the wavefront array, and by using a highly efficient *heap method*, the sorting from minimum to maximum traveltime is carried out promptly. This method was used by Cao and Greenhalgh (1994). Next, we extract the minimum once again, update all neighbouring live gridpoints, and so on. Figure 2 shows schematic plots of the progress of this method along a 2D Cartesian grid.

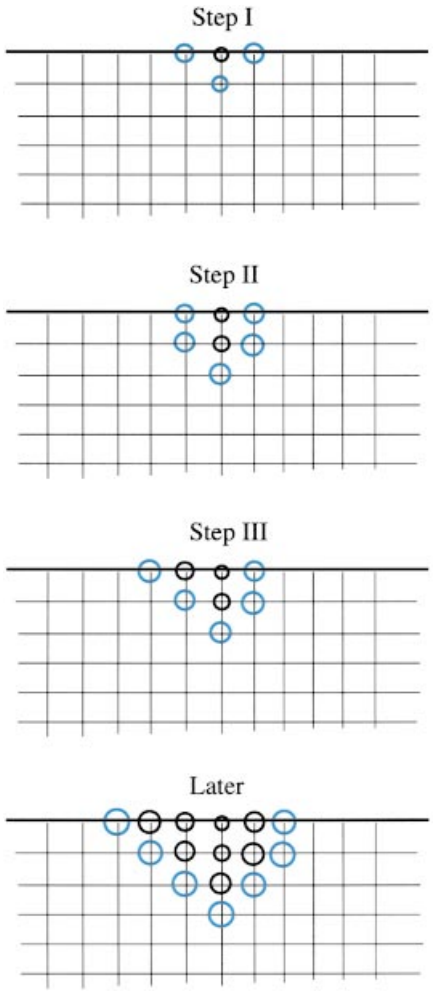

Figure 2 The steps taken to implement fast marching in Cartesian coordinates. Black circles represent computed traveltimes that are set, because of their minimum nature, at the time of extraction from the heap array. Blue circles constitute the front of the wave. They are stored in the wavefront heap array and are sorted from minimum to maximum traveltimes. The traveltime is given schematically by the size of the circle; the larger the radius, the greater the traveltime. The minimum is always extracted first from the heap array at each step, its traveltime is set (given by a black circle), and surrounding gridpoints that are not set are computed and inserted into the wavefront heap array. This process is repeated until all gridpoints are computed and set.

The first-order nature of the fast marching method results in large errors for conventional Cartesian-coordinate sparse gridpoint configurations. In most cases, the largest of these errors occur at the first step of computation. To demonstrate,

let us consider a simple example where the wave slowness is 1 s/km, and the grid spacing is 1 km. In Fig. 3, the gridpoint A is the location of the source and its traveltime is, as a result, set to zero. Gridpoints B and C are part of the wavefront with traveltimes accurately calculated at B and C (both for $t = 1$). Next, gridpoint B is extracted from the wavefront array and used to calculate the traveltime at D based on (4). As a result, the traveltime at D is equal to $1 + \frac{1}{\sqrt{2}}$ instead of the true value of $\sqrt{2}$. This difference corresponds to approximately 20% error in the traveltime calculation at D. This 20% error is always associated with the computation of traveltimes for the first layer of gridpoints regardless of the grid spacing. The smaller the grid spacing, the lesser the impact this error has on the overall calculation of traveltimes away from the source. It is also probably the maximum error allowed by this scheme, which occurs here because of the 45° wavefront propagation angle and the high wavefront curvature (near the source). The next layer of gridpoints should have lower relative errors. If a plane wave (that is, with no curvature) passes through the same gridpoints in Fig. 3 at a 45° wavefront propagation angle, the traveltime at D computed using (4) is equal to $\sqrt{2}$, which is accurate. Therefore the amount of wavefront curvature with respect to the grid is another factor that affects the size of the error. As we propagate away from the source, the percentage error is reduced considerably. One way to avoid errors near the source is to compute the traveltime analytically at gridpoint D and delay starting the fast marching algorithm until after the first group of gridpoints surrounding the source has been computed.

However, such first-order errors will always exist, as will be seen in the numerical examples, regardless of how we compute the initial set of points. One way to reduce such errors, while retaining the main features of the method, is to use the spherical-coordinate system, as is shown in the next section.

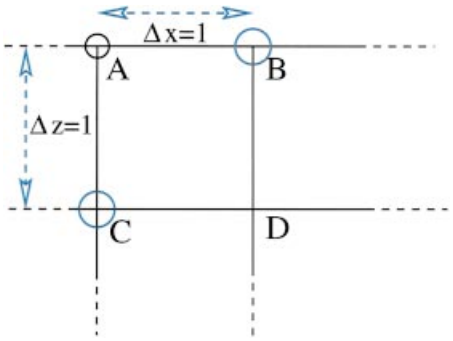

Figure 3 A simple Cartesian-coordinate grid configuration. In this model, the slowness equals 1. Gridpoint A is set, and B is the minimum traveltime along the front that includes B and C. We then compute D as a neighbour of B.

FAST MARCHING IN SPHERICAL COORDINATES

In spherical, or polar, coordinates, waves emanating from a point source are effectively propagating a plane wave on a regular grid. For homogeneous media, this plane wave will have a front that is always parallel to the θ–ϕ plane. As a result, the traveltime calculation using (4) in spherical coordinates is always exact in homogeneous media.

Figure 4 is similar to Fig. 2, but the polar-coordinate system is used. The source is computed initially and set to zero for all angles θ. When stretched on a regular grid, all points on the surface $r = 0$ are set to zero. These points are inserted in the wavefront array and sorted from minimum traveltime to maximum. In the case of the source gridpoint, the sorting step is unnecessary because all traveltimes are equal to zero. The minimum is then extracted and the traveltimes for neighbouring gridpoints are computed using the following relationship:

$$\max(D_{ijk}^{-r}t, 0)^2 + \min(D_{ijk}^{+r}t, 0)^2 + \max(D_{ijk}^{-\theta}t, 0)^2 + \min(D_{ijk}^{+\theta}t, 0)^2 + \max(D_{ijk}^{-\phi}t, 0)^2 + \min(D_{ijk}^{+\phi}t, 0)^2 = s_{ijk}^2, \quad (5)$$

where D_{ijk}^{-r} is the derivative of traveltime with respect to r at gridpoint (i, j, k), given by

$$D_{ijk}^{-r}t = \frac{t_{i,j,k} - t_{i-1,j,k}}{\Delta r}$$

and

$$D_{ijk}^{+r}t = \frac{t_{i+1,j,k} - t_{i,j,k}}{\Delta r}.$$

The D_{ijk}^{θ} and D_{ijk}^{ϕ} derivatives are slightly different, given by

$$D_{ijk}^{-\theta}t = \frac{t_{i,j,k} - t_{i,j-1,k}}{r\Delta\theta},$$

$$D_{ijk}^{+\theta}t = \frac{t_{i,j+1,k} - t_{i,j,k}}{r\Delta\theta},$$

$$D_{ijk}^{-\phi}t = \frac{t_{i,j,k} - t_{i,j-1,k}}{r\sin\theta\Delta\phi}$$

and

$$D_{ijk}^{+\phi}t = \frac{t_{i,j+1,k} - t_{i,j,k}}{r\sin\theta\Delta\phi}.$$

Unlike the implementation in Cartesian coordinates, the

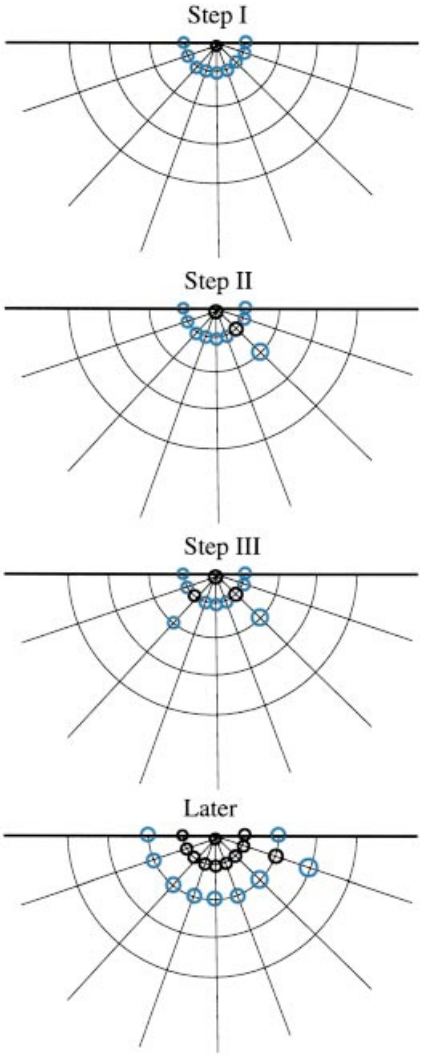

Figure 4 The steps taken to implement the fast marching in polar coordinates. This implementation resembles the Cartesian-coordinate one shown in Fig. 2, but with a different grid orientation. Black circles indicate computed traveltimes that are set because of their minimum traveltime value along the wavefront. Blue circles constitute the wavefront, and their values are ordered in the heap array from minimum to maximum. The minimum is always extracted first from the heap array at each step, its traveltime is set (given a black circle), and all surrounding gridpoints that are not set are computed and put into the heap array.

heap array size in polar coordinates tends to be stable; as we extract a gridpoint, we usually insert another. In Cartesian coordinates, the heap array can become very large, especially in 3D media, as the wavefront expands. Figure 5 shows the size of the heap array for implementing the fast marching method on the model in Fig. 7 using polar coordinates (black curve) and Cartesian coordinates (grey curve). Clearly, the heap array size in polar coordinates is practically the same

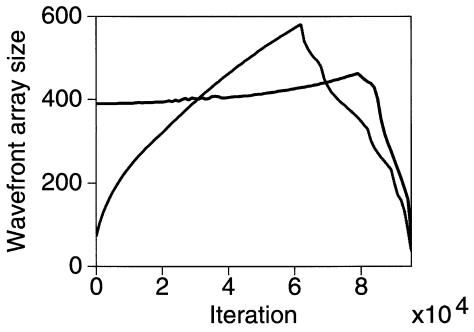

Figure 5 The wavefront heap array size as a function of the number of iterations for traveltimes calculated in the model shown in Fig. 7. The black curve corresponds to the fast marching method using polar coordinates, while the grey curve corresponds to the method using Cartesian coordinates.

through most of the computation, while the Cartesian version grows dramatically and then drops. The increase is greater in 3D media. Using (5), the majority of the errors accumulate when the wave travels diagonally with respect to the coordinate system. Even with the polar-coordinate system, the majority of the errors occur when the wavefront is at a 45° angle to the grid configuration. The time that the wavefront spends travelling diagonally along the polar coordinates is small, even in complex media, relative to that in the Cartesian-coordinate system. Also, the wavefront curvature, another source of error in the scheme, although physically present because of using a point source, does not computationally exist at the start of the wave along the spherical grid. As a result, the errors that accumulate at the start of wavefront propagation in the Cartesian-coordinate system are minimized in the spherical-coordinate implementation.

NUMERICAL TESTS

The numerical examples shown below demonstrate the advantages of using the spherical, or polar, coordinate system, over the Cartesian one, with this new efficient and unconditionally stable eikonal solver. The Cartesian-coordinate implementation includes analytically solving for the first layer of gridpoints around the point source to reduce the wavefront curvature errors.

Figure 6(a) shows the traveltime in a homogeneous medium computed using a second-order in time, or first-order in ray parameters, eikonal solver (van Trier and Symes 1991), incorporating a grid-adaptive scheme (D. Hale 1992, pers. comm.) to achieve better stability. The grid-adaptive approach is based on using a finer polar grid whenever the

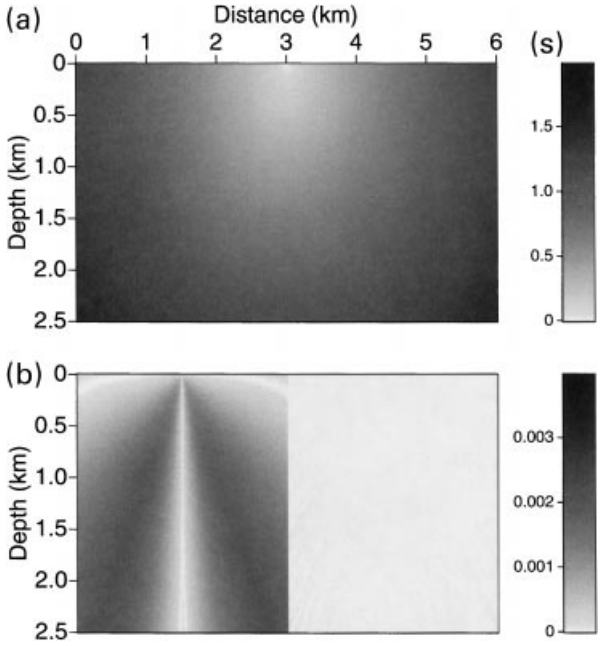

Figure 6 (a) Traveltimes (in seconds) in a homogeneous medium with velocity equal to 2500 m/s, resulting from a source located on the surface at distance 3000 m. (b) The absolute difference, or error, (in seconds) between traveltimes calculated by the fast marching method using Cartesian coordinates (left) and polar coordinates (right) compared with the more accurate second-order eikonal solver. In this homogeneous case, the polar-coordinate fast marching method has practically no errors. Legends of traveltime magnitude in seconds for both plots are shown on the right.

inhomogeneity of the medium dictates it. However, since the approach accommodates refinements of the grid along only the polar coordinate (not all coordinates), it is not an unconditionally stable method. This eikonal solver, because of its higher-order accuracy, serves as a reference for testing the accuracy of the fast marching implementation in different coordinate systems. In addition, this particular second-order solver is exact in homogeneous media, because it is executed in polar coordinates. Figure 6(b) shows the traveltime difference, or error, between implementing the fast marching method in Cartesian coordinates (left) and polar coordinates (right), in contrast to the more accurate second-order scheme. As expected, the majority of the errors in the Cartesian-coordinate implementation are concentrated around the 45° angle wave propagation. The errors also increase more rapidly near the source where the wavefront curvature is greatest. The polar-coordinate fast marching implementation, on the other hand, is almost exact for homogeneous media. In this case, the waves propagate in a plane-wave geometry with respect to the grid orientation.

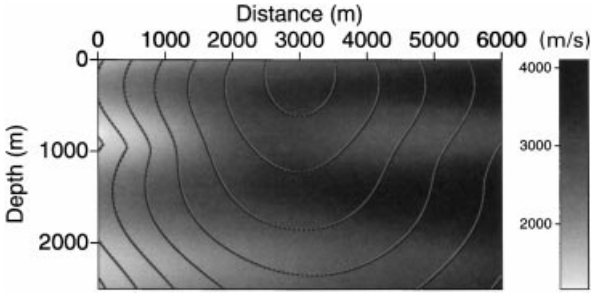

Figure 7 Contours of traveltimes resulting from a source placed on the surface at a distance of 3000 m. The traveltime contours are superimposed on the velocity model (in m/s). The solid black curves correspond to the solution of the more accurate second-order eikonal solver. The grey curves correspond to the use of the fast marching eikonal solver in Cartesian coordinates; the dashed curves, in polar coordinates. The three curves are very similar.

Figure 7 shows traveltimes in a slightly more complicated velocity model. The traveltime contours computed using the various methods practically coincide. A magnified view (Fig. 8) reveals, as in Fig. 6, the details of the errors using the different coordinate schemes. Figure 8(a) shows the result of using the second-order eikonal solver and Fig. 8(b) shows the absolute traveltime errors obtained when using the fast

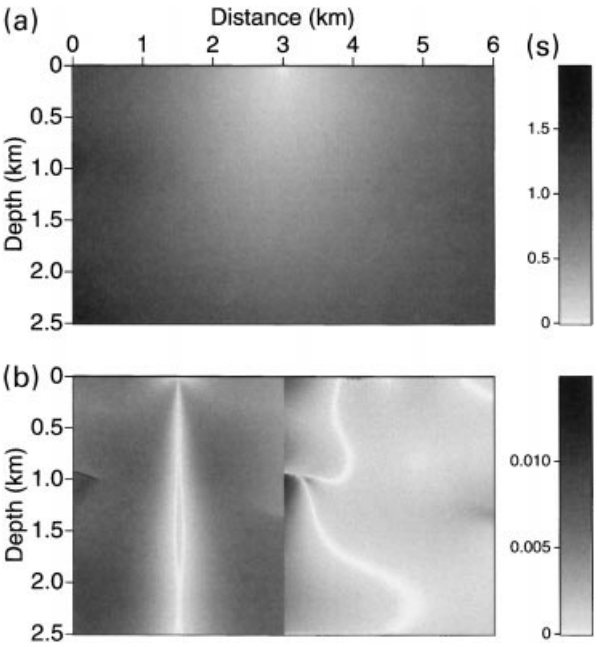

Figure 8 (a) Traveltimes (in seconds) for waves propagating in the model shown in Fig. 7, resulting from a source located on the surface at a distance of 3000 m. (b) The absolute difference, or error, (in seconds) between traveltimes calculated by the fast marching method using Cartesian coordinates (left) and polar coordinates (right) compared with the more accurate second-order eikonal solver.

marching method in Cartesian coordinates (left) and polar coordinates (right). The computational costs of the Cartesian- and polar-coordinate implementations are approximately the same; both methods are far faster than the more accurate second-order scheme. Clearly, the polar-coordinate implementation has far fewer errors than the Cartesian-coordinate one.

THE MARMOUSI MODEL

We used an unsmoothed version of the Marmousi model to test the accuracy and stability of the fast marching method. For comparison, the lateral grid spacing was reduced by half to obtain a more efficient finite-difference solution to the acoustic wave equation. Because the second-order scheme (van Trier and Symes 1991), even with the adaptive measures, is not stable in such a complex model, we used a version of the fast marching eikonal solver, implemented on a very fine grid (one-quarter of the original grid spacing) in polar coordinates to reduce the first-order traveltime derivative errors, in order to generate the reference solution. Thus, the solution of this fine-grid implementation served to test the accuracies of Cartesian- and polar-coordinate implementation of the method on a more practical grid spacing.

Figure 9 shows traveltime contours using the fast marching method in Cartesian coordinates (dashed curves), and in polar coordinates (grey curves). The black curves show traveltimes for the more accurate reference solution based on a fine-grid implementation. The source was placed above a complicated region of the Marmousi, which causes multi-arrival traveltimes. For vertical and horizontal wave propagation, the various contours practically overlap. At a near 45° angular wave propagation, the dashed curves tend to predict faster times than the actual solution. A magnified view (Fig. 10) reveals how much the Cartesian-coordinate implementation hampered the results. The errors are as large as 3% in this area. In some regions, the polar-coordinate implementation may give worse results, for example at distance 2500 m and depth 2000 m, but overall, the fast marching method in polar coordinates gives better results than the Cartesian-coordinate implementation as shown in Fig. 11. Both practical-grid implementations were executed on a 200 MHz Pentium processor and took less than 2 s of computer (CPU) time.

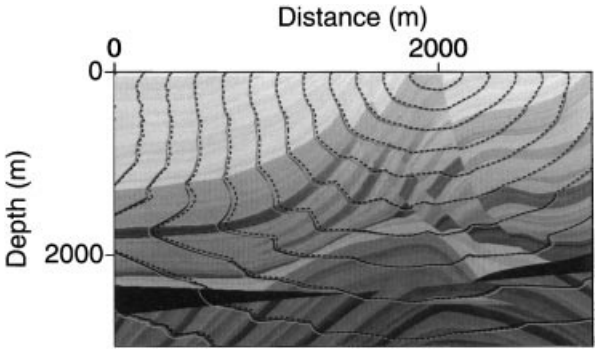

Figure 9 Contours of traveltimes in the Marmousi model resulting from a source placed on the surface above a more complicated region, at a distance of 2000 m. The solid black curves correspond to the solution of the fast marching method using a very fine grid, i.e. the reference solution. The dashed curves correspond to use of the fast marching eikonal solver in Cartesian coordinates; the grey curves, in polar coordinates. While the solid black and grey curves are close overall, the dashed curve corresponding to the Cartesian-coordinate solution again has problems near 45° wave propagation.

Finer grid coverage in the Cartesian-coordinate implementation will reduce such errors, but at a higher computational cost. For the same computational cost as the coarse Cartesian implementation, the polar-coordinate implementation of the fast marching method provides far better results even in complex models.

Figure 12 shows the 0.5 s contour curves superimposed on a snapshot of the finite-difference solution of the acoustic wave equation at time 0.5 s resulting from a source at time zero. The source is above a complicated area of the Marmousi model and some evidence of the departure of the eikonal solution from the most energetic solution appears, especially for waves travelling vertically. A snapshot taken 1 s later (Fig. 13) shows how much the eikonal solution departed from the most energetic solution. This departure results in less than desirable traveltimes when using the eikonal solution for a process such as migration (Geoltrain and

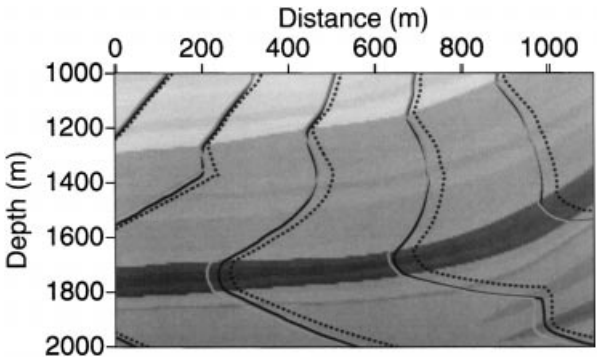

Figure 10 A detail of Fig. 9, demonstrating the accuracy of the polar-coordinate solution given by the grey curves as opposed to the Cartesian one given by the dashed curves. The reference solution is indicated by the black curve.

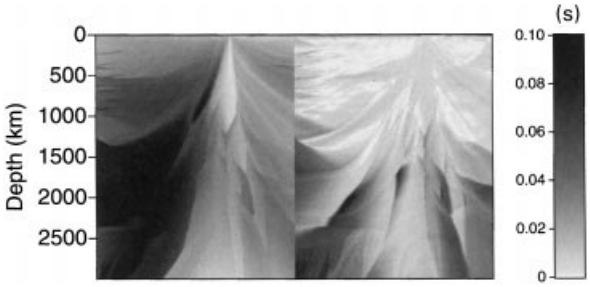

Figure 11 As Fig. 8(b), but for the Marmousi model. The absolute difference, or error, (in seconds) between traveltimes calculated by the fast marching method using Cartesian coordinates (left) compared with polar coordinates (right) and the more accurate, finer grid implementation.

Brac 1993). However, this is the price of such a highly efficient method of calculating traveltimes.

The above examples demonstrate that for an algorithm of the same cost, the accuracy of the polar-coordinate implementation of the fast marching eikonal solver is far superior to the Cartesian version, even in complex models. Both methods are unconditionally stable with no limitations imposed on the direction of the wavefront propagation. Also, while the eikonal solver may provide reasonable solutions in some areas of the Marmousi models, the complexity of other areas results in less than optimal results.

THE SEG/EAGE SALT-DOME MODEL

The accuracy advantages of the spherical-coordinate fast marching eikonal solver also holds for 3D media. We demonstrate this fact on the SEG/EAGE salt-body model.

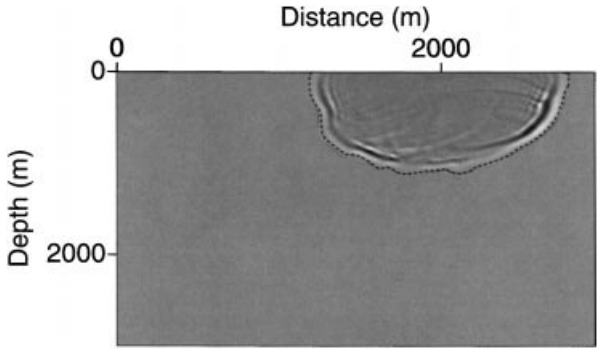

Figure 12 The 0.5 s contour curves from Fig. 9 placed over the finite-difference solution of the acoustic wave equation at time 0.5 s, due to a Ricker wavelet source on the surface at 2000 m distance, discharged at zero time. The contour curves envelop the wave energy at this early time for almost all angles.

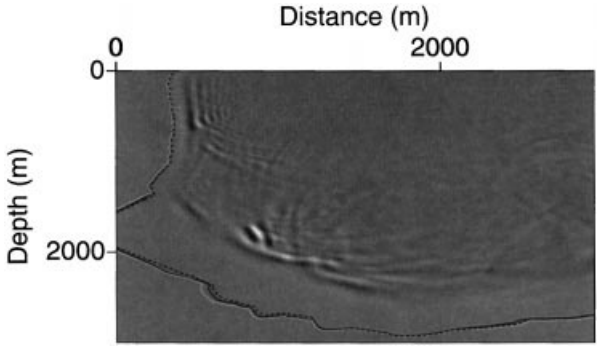

Figure 13 The 1 s contour curves of Fig. 9 placed over the finite-difference solution of the acoustic wave equation at time 1 s, due to a Ricker wavelet source on the surface at 2000 m distance, discharged at zero time. In complex media, the fastest propagating energy is not necessarily the most energetic.

Figure 14 shows the salt structure embedded in two slices of the velocity field outside the salt body. The P-wave velocity in the salt is approximately 4482 m/s. This velocity is much higher than the P-wave velocity in the surrounding sediments, resulting in complicated discontinuities in the P-wavefront (when head waves are excluded). The high-velocity salt body will also result in head waves, as will be seen later, in the eikonal solution in areas where such head waves are the fastest.

Figure 15 shows the salt structure from below with the same two slices that are displayed in Fig. 14. From this view, we can appreciate the complexity of this high-velocity salt structure. Proper imaging of the bottom of the salt reflection requires accurate calculation of the traveltimes through the salt body; it also requires using the proper traveltime arrival (typically the most energetic arrival) in areas of multiple arrivals. Unfortunately, finite-difference solutions of the eikonal equation provide us only with the fastest arrivals, and not necessarily the most energetic ones.

WAVEFRONTS THROUGH THE SALT BODY

To appreciate the effect that the salt body has on wavefronts, we show 3D plots of the wavefront isocrons (constant-traveltime surfaces) as they penetrate the salt body. The complex, yet continuous, wavefronts include body waves, as well as head waves.

Figure 16 shows the eight isocron plots of the wavefront at different times together with either a vertical or depth slice of the velocity field. The wavefront expands with time and its shape alters from the typical spherical shape as it penetrates the salt body. The high salt velocity causes portions of the

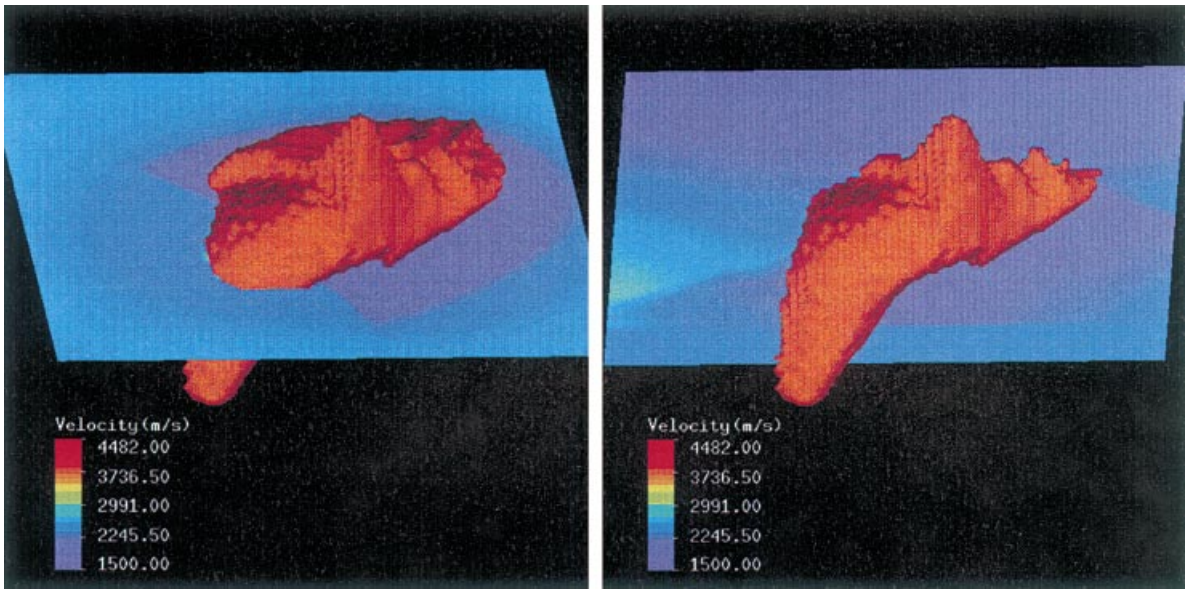

Figure 14 The salt structure displayed from above. The vertical section (left) is the in-line slice through the 3D salt velocity model and the horizontal section (right) is a depth slice through the same velocity model.

wavefront to bulge and expand, especially those parts that have passed through the salt. The top flanks of this bulge are dominated by the head-wave arrivals, which smoothly connect the portions of the wavefront that passed through the salt with those that travelled only through sediments. Clearly, these head-wave flanks have a generally low curvature, especially along the vertical plane, indicative of their low amplitude. The low curvature of head waves in Cartesian coordinates will translate to high curvature in polar coordinates. As mentioned above, propagating high curvature waves is a weakness of the fast marching approach, especially when propagating diagonally with respect to the coordinate system. As a result, head-wave traveltimes, as will be seen below, will include large errors

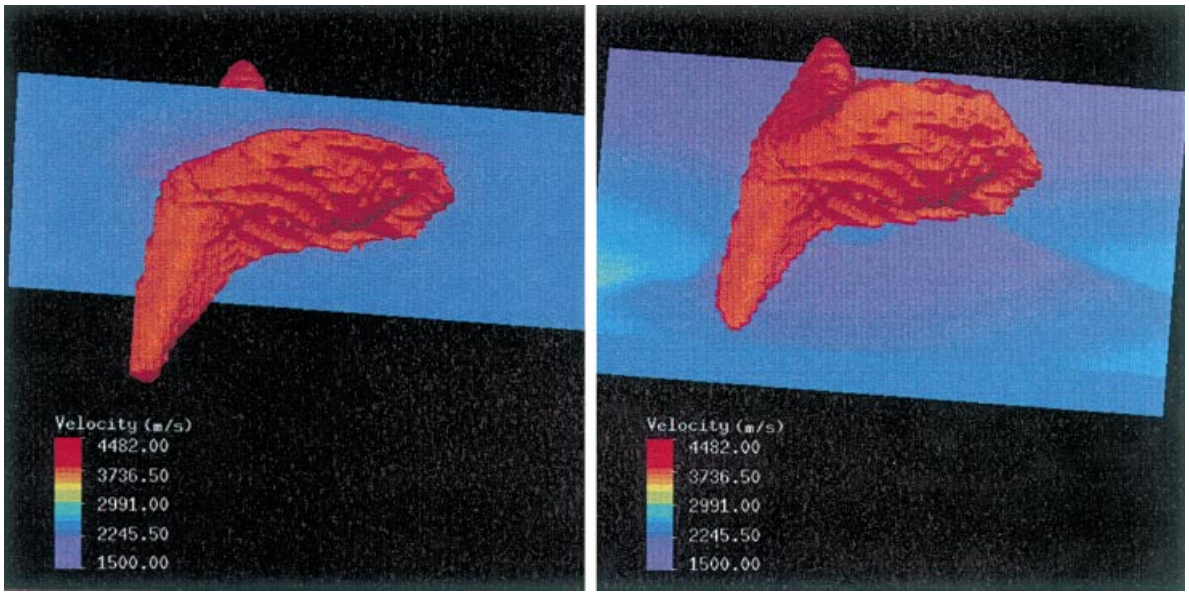

Figure 15 The salt structure displayed from above (left) and from below (right). The vertical section is the in-line slice through the 3D salt velocity model and the horizontal section is a depth slice through the same velocity model.

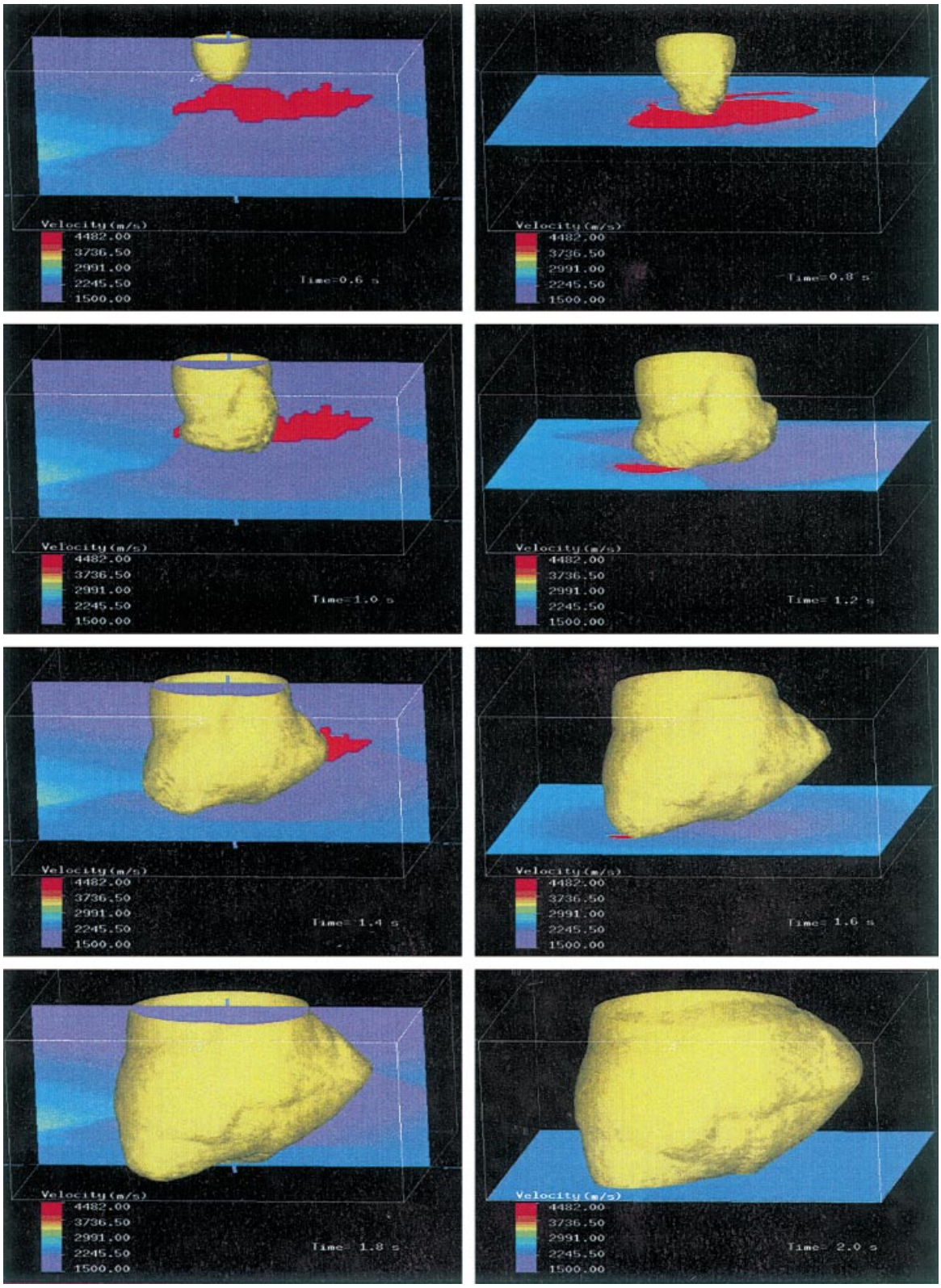
Velocity(m/s)
4482.00
3736.50
2991.00
2245.50
1500.00
Time=0.6 s
Time=0.8 s
Time=1.0 s
Time= 1.2 s
Time= 1.4 s
Time= 1.6 s
Time= 1.8 s
Time= 2.0 s

in the spherical-coordinate implementation of the fast marching method.

The bottom flanks of the wavefronts in Fig. 16 also have low curvature on the vertical plane. This portion of the wavefront corresponds to waves that travelled through the high-velocity salt, and as a result experienced a lot of spreading. These flanks also replace another, but more important, solution of the eikonal equation, i.e. waves travelling directly from the source without going through the salt. These waves, however, arrived a little later, and as a result were excluded from the finite-difference solution of the eikonal equation solution. Such arrivals and their implications will be discussed further in the head waves and first arrivals section.

SPHERICAL VERSUS CARTESIAN

To obtain the eikonal solution using the fast marching method in Cartesian coordinates, we use the conventional fast marching method developed by Sethian and Popovici (1991). For the spherical-coordinate implementation, we use the method developed here. As a reference solution, we solve the spherical version of the fast marching method at a much finer grid, since finite-difference solutions should converge to the exact solution as the grid size approaches zero. The errors here are exaggerated overall because of the relatively large grid spacing used. Specifically, we are solving the eikonal at a grid spacing of 40 m in the x-, y- and vertical z-directions. For spherical coordinates, we use an equivalent spacing that produces results at a comparable time. The reference solution is obtained by using a much finer grid, equivalent to 20 m spacing in all directions.

Figure 17 shows the errors associated with using the fast marching method in Cartesian coordinates. Specifically, we are looking at the traveltime difference between the coarse-grid Cartesian-coordinate implementation and the fine-grid spherical-coordinate implementation. The traveltime errors for such a coarse-grid application are up to 80 ms.

In practice, finer grid configurations are often used to solve the eikonal equation at, of course, a higher price. The finer grid will result in fewer errors (for example 8 ms instead of 80 ms). However, the distribution of the errors and the reason for their presence (the first-order nature of the solution) still apply to finer grid implementation. Such errors are inherent in the method, as was shown above, when certain conditions are met.

Figure 18 shows the errors associated with using the fast marching method in spherical coordinates. Again, we are looking at the traveltime difference between the coarse-grid spherical-coordinate implementation and the fine-grid spherical-coordinate implementation. The traveltime errors for such a coarse-grid application are now up to 60 ms. Unlike the Cartesian-coordinate implementation, most of the errors shown here are associated with low-curvature arrivals, such as head waves. This fact is better demonstrated in Fig. 19, where head waves emanating from the top of the salt are clearly the source of most of the errors associated with the spherical-coordinate implementation. Fortunately, these head-wave arrivals are of low energy, and are generally discarded for imaging applications. In addition, these head waves mask the more important direct-arrival solution.

HEAD WAVES AND FIRST ARRIVALS

Finite-difference solutions of the eikonal equation provide us with continuous wavefront surfaces which correspond to the fastest travelling waves. In the presence of inhomogeneity, such wavefront surfaces might include low-curvature regions corresponding, in some cases, to head waves that often travel faster than the direct waves. Head waves are low-energy arrivals that are not useful for imaging applications (Geoltrain and Brac 1993). The presence of the high-velocity salt body in the SEG/EAGE model has intensified the head waves, and the fast low-energy arrivals problem.

The salt body, because of its very high velocity, acts as a large secondary source that emanates waves from its surface, practically, in all directions. Such waves, typically, have low energy; however, because of their speed through the salt body, they become the fastest arrivals in a major portion of the solution space. Most of these waves appear in the solution of the eikonal equation using finite-difference methods. Some of these waves correspond to head waves; others are simply low-energy solutions. The energy weakness of such waves is a

Figure 16 Eight isocron plots of the wavefront at different times, together with the vertical or horizontal slice of the velocity field. The wavefront corresponds to a wave emanating from the source at the top. The density plots are slices of the velocity field where the salt structure clearly appears in the centre. The vertical velocity slice is kept in the same position, while the horizontal slice of the velocity field is moved along with the wavefront.

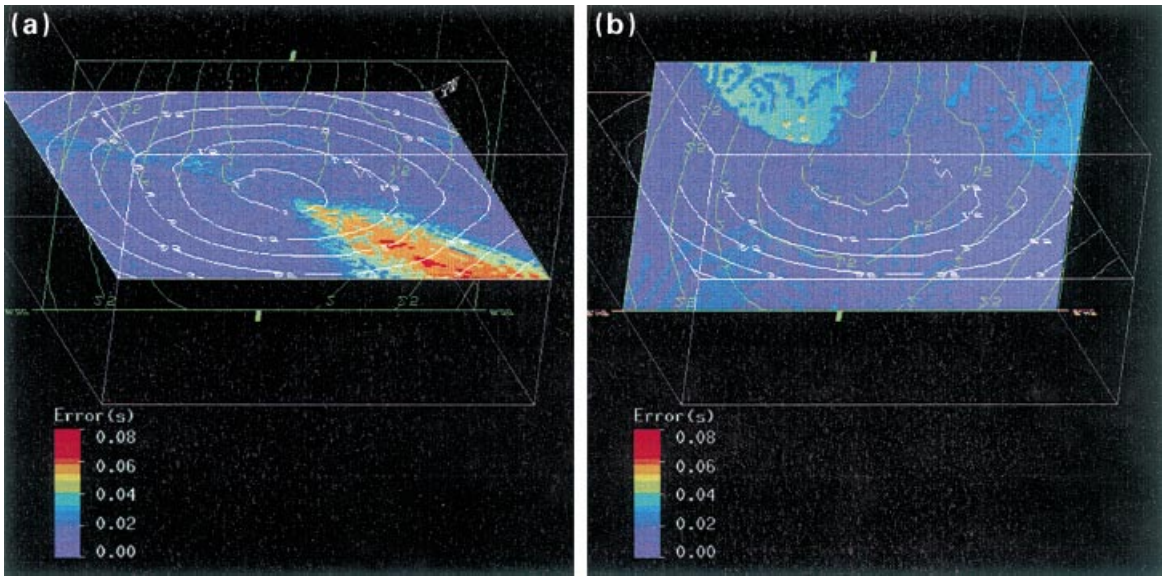

Figure 17 (a) Vertical and (b) horizontal sections of the traveltime errors map that resulted from solving the fast marching method in Cartesian coordinates. Also displayed are the vertical and horizontal sections of the traveltime contour maps.

result of the amount of geometrical spreading they experienced while travelling in the salt body. Typically, the only desired waves propagating through the salt are those that travel downwards to regions not accessible directly by direct waves.

Figure 20 shows two types of low-energy arrival. Figure 20(a) shows head waves emanating from the top of the salt structure. These waves travel partly with the salt wave velocity and thus precede direct arrivals to areas directly above the salt. Figure 20(b) shows another arrival that passed through the salt body and is thus faster than the direct arrivals. The penetration through the salt body, however, has lowered the energy of such arrivals, causing the wavefront to have low curvature.

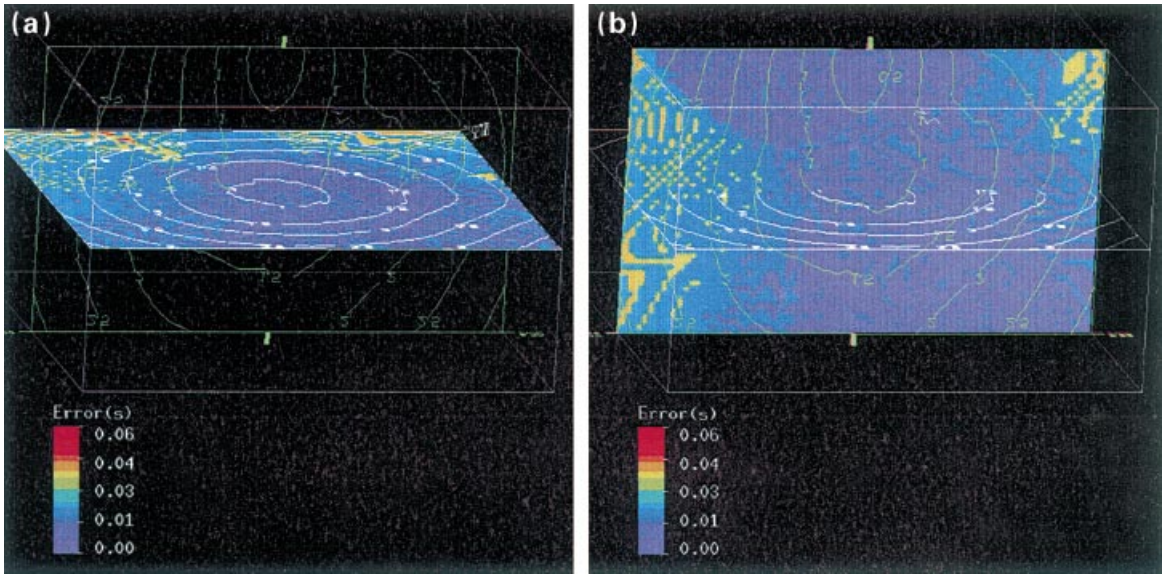

Figure 18 (a) Vertical and (b) horizontal sections of the traveltime errors map that resulted from solving the fast marching method in spherical coordinates. Also displayed are the vertical and horizontal sections of the traveltime contour maps.

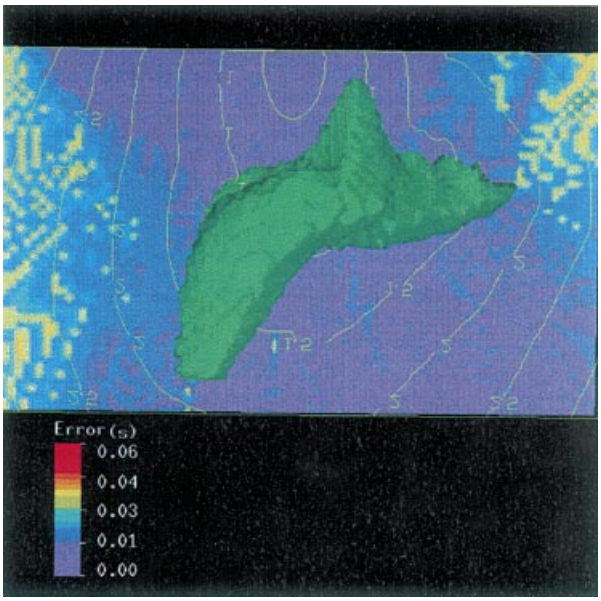

Figure 19 Vertical section of the traveltime contour map that resulted from solving the spherical-coordinate fast marching method superimposed on a slice of the error field associated with the spherical-coordinate implementation (as Fig. 18).

CONCLUSIONS

Spherical coordinates are the most natural orthogonal coordinate system in which to solve the eikonal equation in the case of a point source. The radiation of energy from a point source has an overall spherical shape, even in complex media. The fast marching method of solving the eikonal equation, though fast and unconditionally stable, is based on a first-order approximation of the traveltime derivatives. These approximations yield poor results at 45° angle wave propagation and for highly curved wavefronts. In Cartesian coordinates, such errors accumulate near the source where the curvature of the wavefront is at its highest. For a point source, both the curvature and the 45° angle propagation behaviour are reduced when using polar coordinates. Even in complex media, wavefronts originating from a point source spend less time travelling diagonally with respect to the polar-coordinate system than the Cartesian-coordinate system. The Marmousi model is a prime example of the benefits of the polar-coordinate system for solving the eikonal equation when using the fast marching method.

In addition, for 3D, the fast marching method of solving the eikonal equation is both unconditionally stable and

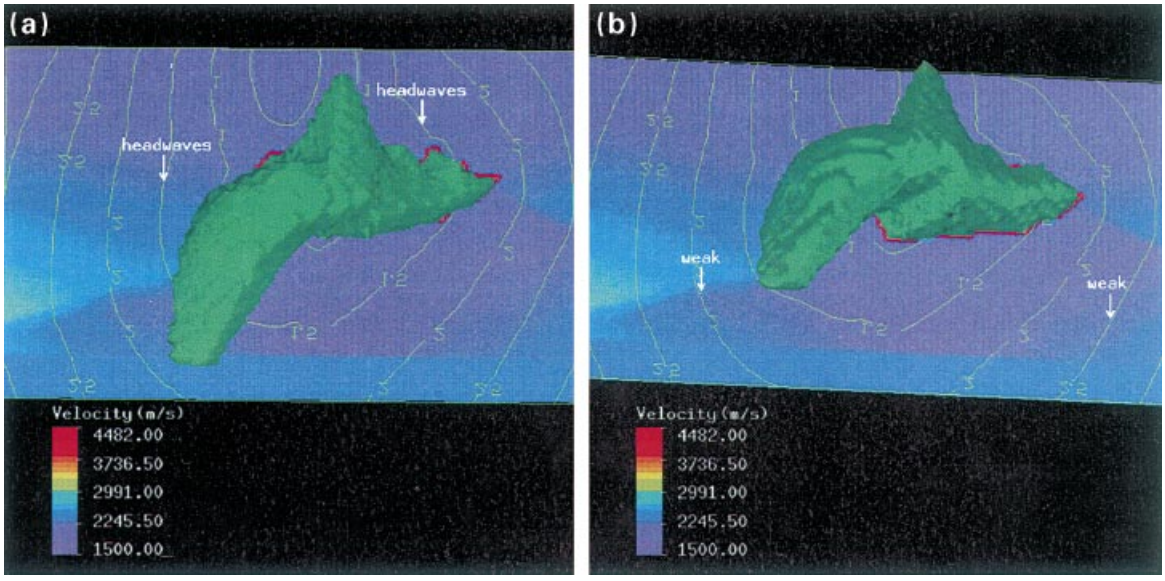

Figure 20 Two-dimensional contour maps of the traveltime with sections of the velocity field displayed in the background and the salt body structure. (a) A semi-top view with the arrow indicating a head wave. (b) A view from below with arrows pointing to the portion of the wavefront that has travelled through the salt, and thus has weak energy. Both waves, because of their first-arrival nature, have replaced the more useful direct waves.

extremely efficient. Both features are well demonstrated on the SEG/EAGE salt-dome model for both the Cartesian- and spherical-coordinate implementation of the fast marching method. However, the spherical-coordinate version provides more accurate direct-wave traveltimes than the Cartesian-coordinate implementation. The only arrivals that suffer in the spherical-coordinate implementation are head waves, which are not useful for imaging.

ACKNOWLEDGEMENTS

T.A. thanks KACST for its financial support, and S.F. thanks the Stanford Exploration Project for its financial and technical support. We also thank the Associate Editor and all reviewers for their review and insightful comments. We especially thank Paul Fowler for his extensive review of the paper.

REFERENCES

Cao S. and Greenhalgh S.A. 1994. Finite-difference solution of the eikonal equation using an efficient first-arrival wavefront tracking scheme. *Geophysics* **59**, 632–643.

Fowler P.J. 1994. Finite-difference solutions of the 3D eikonal equation in spherical coordinates. 64th SEG meeting, Los Angeles, USA, Expanded Abstracts, 1394–1397.

Geoltrain S. and Brac J. 1993. Can we image complex structures with first-arrival traveltime? *Geophysics* **58**, 564–575.

Popovici M. 1991. Finite-difference traveltime maps. *Stanford Exploration Project* **70**, 245–256.

Qin F., Luo Y., Olsen K.B., Cai W. and Schuster G.T. 1992. Finite-difference solution of the eikonal equation along expanding wavefronts. *Geophysics* **57**, 478–487.

Schneider W.A., Jr. 1993. Robust, efficient upwind finite-difference traveltime calculations in 3D. 63rd SEG meeting, Washington, DC, USA, Expanded Abstracts, 1036–1039.

Sethian J.A. 1996. *Level Set Methods*. Cambridge University Press, New York.

Sethian J.A. and Popovici A.M. 1999. Three-dimensional traveltime computation using the fast marching method. *Geophysics* **64**, 516–523.

van Trier J. and Symes W.W. 1991. Upwind finite-difference calculation of traveltimes. *Geophysics* **56**, 812–821.

Vidale J.E. 1990. Finite-difference calculation of traveltimes in three dimensions. *Geophysics* **55**, 521–526.